JPET Fast Forward. Published on June 10, 2022 as DOI: 10.1124/jpet.122.001248
This article has not been copyedited and formatted. The final version may differ from this version.

Nafamostat is a potent human diamine oxidase inhibitor possibly augmenting hypersensitivity reactions during nafamostat administration

Thomas Boehm, Marion Alix, Karin Petroczi, Serhii Vakal, Elisabeth Gludovacz, Nicole Borth, Tiina A. Salminen, Bernd Jilma

Department of Clinical Pharmacology, Medical University of Vienna, Waehringer Guertel 18-20, 1090 Vienna, Austria (T.B., K.P., E.G., B.J.)

Structural Bioinformatics Laboratory, Biochemistry, Faculty of Science and Engineering, Åbo Akademi University, Tykistökatu 6A, 20520 Turku, Finland (M.A., S.V., T.A.S.)

InFLAMES Research Flagship Center, Åbo Akademi University, 20520 Turku, Finland (M.A., S.V., T.A.S.)

Department of Biotechnology, University of Natural Resources and Life Sciences, Muthgasse 18, 1190 Vienna, Austria (E.G., N.B.)

JPET Fast Forward. Published on June 10, 2022 as DOI: 10.1124/jpet.122.001248
This article has not been copyedited and formatted. The final version may differ from this version.

Running title page

Nafamostat is a potent human diamine oxidase inhibitor

Corresponding author

Thomas Boehm

Department of Clinical Pharmacology, Medical University of Vienna

Waehringer Guertel 18-20, 1090 Vienna, Austria

Tel.: +43-1-40400-49580

Fax: +43-1-40400-29980

Email: thomas.boehm@meduniwien.ac.at

ORCID: 0000-0002-8294-0797

Text pages: 15

Number of Tables: 2; Figures: 5

Number of words in the Abstract: 200; Introduction: 800; Discussion: 1600

Abbreviations:

rhDAO	=	Recombinant human diamine oxidase
CPB	=	Cardiopulmonary bypass
ECMO	=	Extracorporeal membrane oxygenator
H_2O_2	=	Hydrogen peroxide
IC_{50}	=	Inhibitory concentration 50%
K_i	=	Inhibitory constant
HRP	=	Horseradish peroxidase
HSA	=	Human serum albumin

Section assignment: Toxicology

JPET Fast Forward. Published on June 10, 2022 as DOI: 10.1124/jpet.122.001248
This article has not been copyedited and formatted. The final version may differ from this version.

Abstract

Nafamostat is an approved short acting serine protease inhibitor. However, its administration is also associated with anaphylactic reactions. One mechanism to augment hypersensitivity reactions could be inhibition of diamine oxidase (DAO). The chemical structure of nafamostat is related to the potent DAO inhibitors pentamidine and diminazene. Therefore we tested whether nafamostat is a human DAO inhibitor. Using different activity assays nafamostat reversibly inhibited recombinant human DAO with an IC_{50} of 300 to 400 nM using 200 µM substrate concentrations. The K_i of nafamostat for the inhibition of putrescine and histamine deamination is 27 nM and 138 nM respectively. For both substrates nafamostat is a mixed mode inhibitor with p-values <0.01 compared to other inhibition types. Using 80% to 90% EDTA plasma the IC_{50} of nafamostat inhibition was approximately 360 nM using 20 µM cadaverine. In 90% EDTA plasma the IC_{50} concentrations were 2-3 µM using 0.9 µM and 0.18 µM histamine as substrate. In silico modeling showed a high overlap compared to published diminazene crystallography data, with a preferred orientation of the guanidine group towards topaquinone. In conclusion, nafamostat is a potent human DAO inhibitor and might increase severity of anaphylactic reaction by interfering with DAO-mediated extracellular histamine degradation.

JPET Fast Forward. Published on June 10, 2022 as DOI: 10.1124/jpet.122.001248
This article has not been copyedited and formatted. The final version may differ from this version.

Significance Statement

Treatment with the short-acting anticoagulant nafamostat during hemodialysis, leukocytapheresis, extracorporeal membrane oxygenator procedures and disseminated intravascular coagulation is associated with severe anaphylaxis in humans. Histamine is a central mediator in anaphylaxis. Potent inhibition of the only extracellularly histamine-degrading enzyme diamine oxidase could augment anaphylaxis reactions during nafamostat treatment.

JPET Fast Forward. Published on June 10, 2022 as DOI: 10.1124/jpet.122.001248
This article has not been copyedited and formatted. The final version may differ from this version.

Introduction

Nafamostat (6-carbamimidoylnaphthalen-2-yl) 4-(diaminomethylideneamino)benzoate; Futhan; Fut-175) is a serine-protease inhibitor of various enzymes such as thrombin, factor Xa, factor XIIa, plasmin or kallikrein (Aoyama et al., 1984; Fuji et al., 1981; Hitomi et al., 1985; Okajima et al., 1995). For several decades it has been used as a treatment for pancreatitis and also as a short-acting anticoagulant for hemodialysis, leukocytapheresis, extracorporeal membrane oxygenator (ECMO) procedures and disseminated intravascular coagulation (Han et al., 2011; Sawada et al., 2016; Minakata et al., 2019). Nafamostat is additionally considered a new treatment option for COVID-19, because it inhibits transmembrane protease serine 2 (TMPSS2), which is involved in SARS-CoV-2 entry into target cells (Hoffmann et al., 2020; Asakura and Ogawa, 2020; Hempel et al., 2021; Yamamoto et al., 2020).

At a steady infusion rate of 0.2 mg/kg/hour nafamostat plasma concentrations reached 90 and 240 nM (Mori et al., 2003). For nafamostat treatment during ECMO a mean dosage of 0.64 mg/kg/hour was used. This would correspond to concentrations between 288 and 768 nM (Han et al., 2011). Some patients received 1.15 to 2.19 mg/kg/hour resulting in plasma concentrations between 518 and 2628 nM. During cardiopulmonary bypass (CPB) 0.2 mg/kg/hour nafamostat were administered before and after CPB, and 2 mg/kg/hour during CBP (Miyamoto et al., 1992; Sakamoto et al., 2014). These high dose infusion rates result in μM nafamostat plasma concentrations. The volume of distribution of nafamostat calculated using five healthy volunteers was 0.36 L/kg or 25.2 liter in a person with 70 kg bodyweight but only 0.08 L/kg in 8 hemodialysis patients (Osono et al., 1991). The lower volume of distribution in hemodialysis patients was attributed to a possible arterial-venous fistula (Osono et al., 1991).

JPET Fast Forward. Published on June 10, 2022 as DOI: 10.1124/jpet.122.001248
This article has not been copyedited and formatted. The final version may differ from this version.

Camostat (4-[2-[2-(dimethylamino)-2-oxoethoxy]-2-oxoethyl]phenyl] 4-(diaminomethylideneamino)benzoate; Foipan) is a related serine-protease inhibitor used for the treatment of chronic pancreatitis and postoperative reflux esophagitis. No cases of anaphylaxis have been associated with camostat, but this may be because it is used much less frequently compared to nafamostat, and also because it is not used during extracorporeal circulation treatment. Camostat is only a precursor and is rapidly degraded in the liver to the active 4-(4-guanidinobenzoyloxy)phenylacetic acid (Midgley et al., 1994).

Several reports of nafamostat-induced anaphylactic reactions have been published in patients undergoing hemodiafiltration (Maruyama et al., 1996; Ookawara et al., 2018; Kim et al., 2016; Kim et al., 2021). When compared to that demonstrated by heparin, the adverse reaction profile during leukocytapheresis, showed increased rates of "typical" histamine-mediated symptoms such as headache, nausea, rash, itching, palpitations, dyspnea and anaphylactic shock (Sawada et al., 2016). Miyamoto et al. (1992) measured increased histamine concentrations during CBP using high dose nafamostat and suggested that nafamostat might be a diamine oxidase (DAO) inhibitor.

Human DAO (E.C. 1.4.3.22) is a copper-containing amine oxidase that oxidatively deaminates histamine and various polyamines releasing ammonia and hydrogen peroxide (Elmore et al., 2002). In humans, high DAO mRNA levels and enzymatic activity were measured in the gastrointestinal tract with increased concentrations in the duodenum and ileum/jejunum compared to the colon. Additionally, high levels were found in the proximal tubular epithelial cells of the kidneys and in the extravillous trophoblast cells, fetal cells invading the decidua and the myometrium during placenta development (Elmore et al., 2002; Schwelberger et al., 1998a; Schwelberger et al., 1998a; Velicky et al., 2018). Plasma DAO concentrations increase at least 100-fold during pregnancy (Southren et al., 1964; Boehm et al., 2017). In two large animal studies involving pigs and sheep, irreversible pharmacological

JPET Fast Forward. Published on June 10, 2022 as DOI: 10.1124/jpet.122.001248
This article has not been copyedited and formatted. The final version may differ from this version.

inhibition of DAO activity using high doses of aminoguanidine resulted in increased morbidity and mortality after exogenous histamine challenge (Sattler et al., 1988; Sjaastad, 1967). Nevertheless, the role of DAO in the elimination of endogenous histamine during anaphylaxis or during mast cell activation is not clear.

The symmetrical diamidines, pentamidine and diminazene, are potent DAO inhibitors (McGrath et al., 2009; Duch et al., 1984). Although nafamostat is not a classic diamidine and is not symmetrical, it could be a potent DAO inhibitor because it contains one terminal amidinium and one terminal guanidinium moiety, in addition to a naphthyl group. Two of the most potent DAO inhibitors, isometamidium and prothidium, contain a phenanthridine triple aromatic ring structure and two additional individual aromatic rings (Duch et al., 1984). The marginally less active antricyde is composed of a quinoline group, a double aromatic ring like naphthalene, and a benzyl ring (Duch et al., 1984). For efficient DAO inhibition, aromatic ring structures in combination with terminal amidinium/guanidinium moieties and several nitrogen atoms are clearly important. Amiloride contains seven nitrogen atoms and a pyrazine aromatic ring, but is a much weaker DAO inhibitor compared to phenamil or benzamil, which carry a second aromatic ring, phenyl or benzyl group respectively, linked to the guanidinium moiety of amiloride (Novotny et al., 1994).

If DAO is potently inhibited by nafamostat, endogenous histamine degradation might be impaired during nafamostat administration, possibly augmenting hypersensitivity reactions. In a first step towards answering this clinically relevant question, we tested whether nafamostat is a bona fide human DAO inhibitor.

JPET Fast Forward. Published on June 10, 2022 as DOI: 10.1124/jpet.122.001248
This article has not been copyedited and formatted. The final version may differ from this version.

Materials and methods

References used only in the Material and Methods section are listed in the Supplement. In this section only numbers are assigned. If the reference is also used in other sections, it is regularly listed with name and year.

Chemicals and reagents

Albunorm (Octapharma, Vienna, Austria), a 20% human serum albumin (HSA) solution, is authorized for human use and 96% of the protein content is HSA. Its other ingredients, 16.8 mM caprylic acid and 16.8 mM N-acetyl-tryptophan, do not inhibit DAO activity. Phosphate buffered saline (PBS) pH 7.4 without $MgCl_2$ and $CaCl_2$ was purchased from Gibco (Vienna, Austria). Diminazene aceturate (D7770), DMSO (D2650), putrescine (P5780), cadaverine (C8561), histamine (53300), ortho-aminobenzaldehyde (A9628), horse radish peroxidase (HRP; P6782), amiloride (A7410), benzamil (B2417), phenamil (P203), camostat (SML0057), sodium fluoride (201154), phenylhydrazine (114715), methylhydrazine (M50001), 2-hydroxyquinoline (270873), glucose oxidase (G6125), ethyl acetate (34858), DNTB (Ellman's reagent; D8130), vanillic acid (94770), 4-aminoantipyrine (33528) were purchased from Sigma-Aldrich (Vienna, Austria). Nafamostat was purchased from Torii Pharmaceuticals (Futhan) and Cayman (14837; Vienna, Austria). Aminoguanidine (81530) was bought from Cayman. Foipan tablets and 5% glucose solution were provided by the pharmacy at the General Hospital Vienna. Naphthalene-2-yl-benzoate (330610050) and Amplex red (12222) were purchased from Thermo Fisher Scientific (Vienna, Austria). If not otherwise indicated compounds were dissolved in DMSO at 10 mM and stored at -32°C for no longer than 2 years, or were freshly prepared and used immediately. Foipan tablets were ground and dissolved in DMSO or water at a 10 mM camostat concentration. The DMSO

JPET Fast Forward. Published on June 10, 2022 as DOI: 10.1124/jpet.122.001248
This article has not been copyedited and formatted. The final version may differ from this version.

solution was clear and used immediately. The water solution was centrifuged at high speed for 5 min and the supernatant was assumed to contain 10 mM camostat.

DAO activity assay using hydrogen peroxide (H_2O_2) horseradish peroxidase (HRP) coupling with luminol, Amplex red or vanillic acid/4-aminoantipyrine

The luminol DAO activity assay is based on a published luminescence assay (Supp. Ref. 1) and is described in detail (Boehm et al., 2020). The expression and purification of recombinant human (rh)DAO in Chinese hamster ovary cells has been previously published (Supp. Ref. 2). Final DAO concentrations were 0.2 to 1 µg/ml (1.2 to 6 nM based on the dimer and excluding the molecular weight of the extensive glycosylation), quantified using absorption measurements or using an in-house developed DAO ELISA (Boehm et al., 2017). For activity assays we used 0.05% to 0.1% HSA PBS buffer or 80 to 90% plasma from healthy volunteers as matrix. The pH of the luminol solution from a commercial ECL western blotting kit (Amersham RPN2106, Vienna, Austria) was adjusted from 9.2 to 8.0. The lower pH is closer to a physiologically relevant pH level and the quantum yield is still sufficiently high to effectively measure DAO activity.

Using 50 µM Amplex red instead of luminol allows H_2O_2-HRP coupling in HSA PBS buffer with higher sensitivity. It also allows for easier oxidation rate calculations because the assay can be performed using continuous measurements with accumulating stable resorufin (Boehm et al., 2020).

We also used H_2O_2-HRP vanillic acid/4-aminoantipyrine coupling as described (Supp. Ref. 3). The chromophore measured at 490 nm is relatively pH insensitive between pH 6 and pH 10. This assay was also used to measure the potency of nafamostat between pH 6 and 10 using the Britton-Robinson buffer system with 0.1% HSA (Supp. Ref. 4).

DAO activity assay using p-dimethylaminomethylbenzylamine oxidation

JPET Fast Forward. Published on June 10, 2022 as DOI: 10.1124/jpet.122.001248
This article has not been copyedited and formatted. The final version may differ from this version.

The presence of antioxidants or other molecules interfering with H_2O_2-HRP coupling distort proper DAO activity measurements [32]. Dimethylaminomethylbenzylamine is a substrate for DAO, which can be directly quantified. However, the K_m is only 110 µM or approximately 5.5- to 39-fold higher compared to putrescine and histamine respectively (Elmore et al., 2002; Boehm et al., 2020). We used a benzaldehyde extinction coefficient of 11000 $M^{-1}cm^{-1}$ at 250 nm for rate calculations. This value is about 100-fold higher compared to the benzylamine moiety of the parent compound. UV-compatible 96 well half-area plates (UltraCruz™ UV plates, SCBT, Heidelberg, Germany) were utilized. A HSA concentration of 0.05% reduced the protein-based signal at 250 nm to acceptable levels.

DAO activity assay using fluorescence measurements

Diamine oxidase generates delta-1-piperideine (2,3,4,5-tetrahydro-pyridine), the autocyclized reaction product, using cadaverine as substrate. The condensate between delta-1-piperideine and ortho-aminobenzaldehyde (oABA; stored at -32 °C for 4 to 6 months as a 200 mM stock solution in absolute ethanol) generates 5,5a,6,7,8,9-hexahydropyrido[2,1-^{b}]quinazoline-10-ium or abbreviated HHPQ [32]. Absorption and fluorescence measurement procedures of HHPQ using a Synergy™ H1 Multi-Mode Microplate reader (BioTek; Winooski, Vermont, US) have been published (Boehm et al., 2020).

For the detection of HHPQ in plasma from healthy volunteers we mixed 85 µl plasma adjusted to pH 7.4 with 11 µl 1 M HCl per ml of plasma with 5 µl 10% ethanol or 5 µl 20 mM oABA and 5 µl PBS or 5 µl 4 mM cadaverine and 5 µl 20-fold concentrated inhibitors. Only 80 µl plasma was used testing in addition the influence of esterase inhibitors. All samples were analyzed in duplicate. After incubation for 30 min to 1 hour at 37°C in the dark, 200 µl 7.5% TCA (99.5% trichloroacetic acid; 91228; Sigma-Aldrich; Vienna, Austria) was added and the solution incubated on ice for 20 min. After 10 min of high speed centrifugation, 150 to 200 µl were recovered and fluorescence was measured as described (Boehm et al., 2020).

JPET Fast Forward. Published on June 10, 2022 as DOI: 10.1124/jpet.122.001248
This article has not been copyedited and formatted. The final version may differ from this version.

Measurement of histamine concentrations

Histamine concentrations were measured using the homogenous time resolved fluorescence (HTRF) histamine dynamic kit (62HTMPEG) from Cisbio (now Perkin Elmer) according to the instructions. However, the concentration range was adjusted to the spiked histamine concentrations. Additionally, a standard curve using in-house histamine was utilized, rather than the histamine provided in the kit. Dilutions were selected to measure less than 10 ng/ml (90 nM) histamine, because the slope of the standard curve is steeper improving measurement precision below this concentration. The assays were performed in 20 µl using low volume Cisbio plates (66PL96001) and measured using custom fluorescence filters (EX 330/80; EM 620/10 and EX 330/80; EM 665/8). Plasma was diluted using plasma sample diluent from Cisbio (62DLPDDD).

Irreversible DAO inhibition assay

Diamine oxidase was immobilized onto high protein binding black fluorescence microtiter plates using a monoclonal antibody against human DAO. This process has previously been described for the development and characterization of a human DAO ELISA (Boehm et al., 2017). After washing, 0.1% HSA PBS containing a final concentration of 10 µM of the tested inhibitors was added, and the wells incubated for 30 min at 37°. After this, the wells were washed as described in the DAO ELISA protocol (Boehm et al., 2017). Hydrogen peroxide-HRP Amplex red coupling, the most sensitive DAO activity assay, was used to measure the remaining DAO activity over 2 hours at 37°C.

Kinetic analysis

The H_2O_2-HRP Amplex red coupling assay was used for kinetic analysis. Putrescine was tested between 5 and 80 µM and histamine between 0.63 and 10 µM. All samples were tested in duplicate and the mean was used for further calculations. For both substrates a DAO

JPET Fast Forward. Published on June 10, 2022 as DOI: 10.1124/jpet.122.001248
This article has not been copyedited and formatted. The final version may differ from this version.

concentration of 200 ng/ml (1.2 nM) was used. Diamine oxidase activity of the different nafamostat and substrate combinations was determined using the linear part of the slope of the increasing fluorescence signal. The coefficient of determination (R^2) of the used part of the curve was consistently above 98%. Statistical kinetic analysis was performed using GraphPad Prism.

In silico prediction of nafamostat binding to DAO

The docking preparations and experiments were performed using Maestro 2019-4 (Supp. Ref. 5-8). The DAO structure in complex with diminazene, which is also the best resolution structure of DAO in the Protein Data Bank (PDB 3HIG), was prepared using the Protein Preparation Wizard (Supp. Ref. 9). Nafamostat and diminazene were prepared using LigPrep (Supp. Ref. 9). Nafamostat and diminazene dockings were performed with Glide by defining the grid in the centroid of diminazene in the B chain of the DAO crystal structure. The performance of the docking program and the best parameters (the centroid of diminazene was used as the centroid of the grid, no constraints and flexible ligand) were tested using control docking with diminazene. The control docking resulted in 6 diminazene poses (docking scores between 9.131 and -8.267) identical to the DAO/diminazene crystal structure (PDB ID 3HIG, Supp. Fig. 7). It also resulted in 21 similar poses among a total of 48. The same parameters were used for nafamostat docking. The interaction maps were created using the Protein–Ligand Interaction Profiler PLIP (Adasme et al., 2021). The Molecular Mechanics Generalized Born Surface Area (MMGBSA) binding energy was calculated for the diminazene/DAO complex structure (PDB ID 3HIG) and for the two best nafamostat poses obtained in the docking study (Supp. Ref. 10, 11). All figures were prepared using the PyMOL Molecular Graphics System, Version 2.4.1, Schrödinger, LLC.

Ethics

The study numbers for the collection of plasma samples from healthy volunteers are EC:2030/2013 and EC:1810/2015. All healthy volunteers provided their informed consent prior to blood samples being collected. All procedures were performed in accordance with the ethical standards of the responsible committee on human experimentation (institutional and national) and with the Helsinki Declaration of 1975 (revised 2013).

JPET Fast Forward. Published on June 10, 2022 as DOI: 10.1124/jpet.122.001248
This article has not been copyedited and formatted. The final version may differ from this version.

Results

Nafamostat is a potent recombinant human DAO inhibitor

Using luminol with H_2O_2-HRP coupling the IC_{50} of nafamostat for DAO inhibition is 407 nM. This is comparable to phenamil, a known DAO inhibitor (Fig. 1A) (Novotny et al., 1994). The IC_{50} of nafamostat inhibition using vanillic acid/4-aminoantipyrine H_2O_2-HRP coupling is 341 nM (Supp. Fig. 2C). Nevertheless, potential DAO inhibitors with antioxidant activity might trap radicals released by HRP, interfering with the assay validity. We therefore tested interference of nafamostat using detection of H_2O_2 released from glucose oxidase. It is unlikely that nafamostat is a potent glucose oxidase inhibitor. Nafamostat did not block glucose oxidase activity, thus demonstrating that there is no antioxidant activity (Supp. Fig. 2A). We also measured direct conversion of the artificial DAO substrate p-dimethylaminomethylbenzylamine to the respective aldehyde using absorption rate changes at 250 nm (Bardsley et al., 1972). The obtained data were comparable to H_2O_2-HRP coupling (Fig. 1B). Finally, fusion of deaminated autocyclized cadaverine, delta-1-piperideine, with ortho-aminobenzaldehyde (oABA) was quantified. This was performed both without and in the presence of different nafamostat concentrations. The IC_{50} was 317 nM (Fig. 1C). Camostat or Foipan tablets dissolved in water or DMSO were at least 5-times less potent compared to nafamostat and therefore camostat was not further pursued as a DAO inhibitor (Fig. 1D). Camostat is a pro-drug and the active metabolite is likely less active compared to the parent compound.

The data from three different DAO activity assays characterize nafamostat as a potent direct DAO inhibitor excluding relevant assay interferences possibly explaining DAO inhibition.

JPET Fast Forward. Published on June 10, 2022 as DOI: 10.1124/jpet.122.001248
This article has not been copyedited and formatted. The final version may differ from this version.

Nafamostat is a reversible DAO inhibitor, whose potency is pH independent at physiological pH levels

All known irreversible DAO inhibitors like phenylhydrazine, methylhydrazine or aminoguanidine possess a terminal hydrazine group covalently binding to the highly reactive topaquinone in the active center of DAO (Janes et al., 1992; McGrath et al., 2010). Although the potent DAO inhibitor diminazene aceturate carries an endogenous hydrazine group, it is a reversible DAO inhibitor (McGrath et al., 2009). Nafamostat does not have a hydrazine group. Nevertheless, tryptase is slowly irreversibly inhibited by nafamostat (Aoyama et al., 1984; Fujii et al., 1981). Nafamostat (and camostat) inhibition of the transmembrane protease serine 2 (TMPRSS2), involved in the cellular entry of SARS-CoV-2, seems covalent (Hempel et al., 2021). Therefore we tested whether nafamostat is an irreversible DAO inhibitor.

After washing microtiter plates with immobilized DAO, DAO activity after preincubation with 10 µM nafamostat was equivalent to wells without the addition of an inhibitor. The two hydrazine derivatives showed strong continuous DAO inhibition after the washing step, although irreversibility is not stable and DAO activity is slowly recovering (Fig. 2A). The potent DAO inhibitor diminazene rapidly dissociated from the active center and DAO activity was immediately restored to control values after washing the wells (Fig. 2A and B). These results strongly argue against irreversible DAO inhibition by nafamostat.

The Chemicalize software (ChemAxon) calculated a pKa of 7.6 and 8.5 for the guanidine moiety of nafamostat and camostat respectively (data not shown). This is unusually low for a guanidine group, because guanidine shows a pKa of 12.5, similar to amidine. We therefore tested pH-dependent DAO inhibition of nafamostat using the Britton Robinson buffer system. If a double-protonated nafamostat molecule is important for inhibition, relative DAO inhibition at pH 6.0 should be stronger when compared to pH 8.0. If a single-protonated nafamostat is a better relative DAO inhibitor, nafamostat should be more potent at higher pH

JPET Fast Forward. Published on June 10, 2022 as DOI: 10.1124/jpet.122.001248
This article has not been copyedited and formatted. The final version may differ from this version.

values. The data presented in Fig. 2C demonstrate that the pKa of the guanidine moiety is higher than 9.0. Relative DAO inhibition is constant between pH 6 and 8 and decreases afterwards. This pattern is congruent with a pKa of 9.6 but not 7.6 (Fig. 2D). The pH dependent DAO activity pattern is equivalent to published data (Elmore et al., 2002).

Nafamostat is a mixed mode DAO inhibitor

In the next experiments we employed kinetic analysis using different nafamostat concentrations combined with various histamine and putrescine substrate levels 3- to 4-fold below and above the published K_m values. The published K_m values presumed to be most reliable are 20 and 2.8 µM for putrescine and histamine respectively (Elmore et al., 2002). We obtained nafamostat inhibition constant K_i values of 27 nM and 138 nM for putrescine and histamine respectively (Fig. 3A and 3B). The ratio of the K_m to the K_i of putrescine is 741 and the equivalent histamine ratio just 20. The 37-fold difference between putrescine and histamine suggests that nafamostat is a more potent DAO inhibitor using the lower affinity substrate putrescine compared to the higher affinity substrate histamine. The K_i ratio histamine to putrescine of 5.1 is similar to the K_m ratio of 7.1. The corresponding V_{max} and K_m data, including the standard errors at different nafamostat concentrations, are shown in Fig. 3C and 3D. At low nafamostat concentrations the K_m values for putrescine and histamine increase 7.1- and 8.4-fold per µM increase in nafamostat (data not shown). The IC_{50} values dependent on the substrate concentrations are shown in Fig. 3E and 3F. Based on changing K_m and V_{max} values nafamostat is likely a mixed mode inhibitor. This hypothesis was substantiated by comparing different models of inhibition using the extra sum-of-squares F test, the most appropriate test to identify the mode of inhibition according to the GraphPad manual. These data and additional parameters obtained from kinetic analysis are summarized in Table 1.

Human plasma shifts the inhibitory potency of nafamostat

JPET Fast Forward. Published on June 10, 2022 as DOI: 10.1124/jpet.122.001248
This article has not been copyedited and formatted. The final version may differ from this version.

The kinetic data imply that the assay substrate concentration will have a significant influence on the potency of nafamostat to inhibit DAO activity. Normal histamine concentrations are below 1 ng/ml (9 nM) (Kaliner et al., 1982). The mean histamine concentration during severe anaphylaxis following insect sting challenge was 140 ng/ml or 1.3 µM (Van der Linden et al., 1982). The other known natural substrates of DAO are the polyamines putrescine, spermidine and spermine, with K_m values of 20 µM, 1100 µM and > 3000 µM respectively (Elmore et al., 2002). Nevertheless, the plasma or serum concentrations of these three polyamines are below 1 µM combined, and are unlikely to significantly interfere with DAO inhibition by nafamostat (Russell, 1983).

Giardina et al. (2018) showed that at 1 nM tryptase 10% and 20% of human plasma shifts the IC_{50} values of a bivalent serine protease inhibitor 1.6- and 2.6-fold respectively. Linear extrapolation to 100% plasma would cause an 8-fold shift in the IC_{50} (Supp. Fig. 6). The mechanism responsible for this shift was not elucidated. We used DAO at 1.2 to 6 nM (0.2 to 1 µg/ml) in our experiments. Finally, stability of nafamostat could influence the potency to inhibit DAO in plasma. Nafamostat is possibly hydrolyzed by esterases with a half-life of approximately 40 minutes using 100 µM nafamostat starting concentration and a rate of 6.5 µM/min, but a low K_m of 8.9 mM (Yamaori et al., 2006). At lower nafamostat concentrations the rate is likely to be significantly reduced. Addition of 1 mM Ellman's reagent or DNT (5,5'-dithiobis(2-nitrobenzoic acid)) to plasma inhibited degradation of 500 µM nafamostat by 83% (Yamaori et al., 2006). The responsible esterase was not identified. In the following experiments we attempted to address two main questions. First, is the inhibitory potency of nafamostat reduced using the complex matrix plasma and second, do esterase inhibitors increase the potency of nafamostat by blocking degradation using 80 to 90% plasma?

The highly sensitive H_2O_2-HRP Amplex red coupling assay cannot be used in plasma or serum because of the high antioxidant capacity of these complex matrices (Boehm et al.,

JPET Fast Forward. Published on June 10, 2022 as DOI: 10.1124/jpet.122.001248
This article has not been copyedited and formatted. The final version may differ from this version.

2020). Using the recently published sensitive fluorescence assay to measure DAO activity in complex matrices like plasma or tissue extracts we were able to reduce the substrate concentration from 200 µM to 20 µM cadaverine (Supp. Fig. 3). The IC_{50} in 85% plasma shifted from 2.3 µM to 386 nM, a 6-fold drop, after reducing cadaverine 10-fold from 200 to 20 µM, (Fig. 4A) (Boehm et al., 2020). Lower substrate concentrations cannot be used because of assay sensitivity limitations. Addition of 1 or 2 mM DNT did not influence the IC_{50} values of DAO inhibition by nafamostat (Fig. 4B). Camostat is also hydrolyzed by plasma esterases and sodium fluoride inhibited camostat degradation (Midgley et al., 1994), but no effect was measured using 40 mM NaF in our assay (Supp. Fig. 5B). We also tested 2-hydroxyquinoline (2HQ), a potent arylesterase inhibitor (Khersonsky and Tawfik, 2005), but did not see any effect on DAO inhibition (Supp. Fig. 5B). Finally, we reasoned that high concentrations of naphthalen-2-yl benzoate (NAPB) might occupy the responsible enzymes potentiating nafamostat inhibition. Naphthalen-2-yl benzoate corresponds to nafamostat without both the terminal amidinium and guanidinium moieties. Diamine oxidase inhibition was not increased using 1 mM NAPB (Supp. Fig. 5A). The influence of the different (aryl)esterase inhibitors on DAO activity measurements was within acceptable boundaries (Supp. Fig. 4).

Although the IC_{50} values shifted 6-fold after reducing the substrate concentrations from 200 to 20 µM cadaverine, the IC_{50} values were still at least 10-fold higher compared to the K_i of 27 nM for putrescine. In general, putrescine and cadaverine behave very similarly as DAO substrate. We also tested 0.9 µM (100 ng/ml) and 0.18 µM (20 ng/ml) histamine substrate concentrations and the IC_{50}s were approximately 2 to 3 µM, which is 15- to 22-fold above the K_i of 138 nM (Fig. 4D). Lower histamine concentrations cannot be accurately quantified, because plasma must be diluted to avoid matrix effects. No histamine degradation was

JPET Fast Forward. Published on June 10, 2022 as DOI: 10.1124/jpet.122.001248
This article has not been copyedited and formatted. The final version may differ from this version.

measured without addition of DAO (data not shown) and endogenous histamine was below 10 nM (data not shown).

In silico docking predicts nafamostat binding to DAO similar to diminazene

Crystal structures of two potent diamidine-type DAO inhibitors, pentamidine and diminazene, complexed with DAO have been published (PDB IDs 3HII, 3HIG). Both are mixed mode inhibitors similar to nafamostat, which may use similar amino acids for tight binding. Nevertheless, nafamostat is not a strict diamidine because it carries a terminal amidinium and a terminal guanidinium moiety. Unlike diminazene and pentamidine it is not symmetrical because it contains a single naphthalene double aromatic ring structure linked to the terminal amidine group (Supp. Fig. 1). Therefore, it is possible that nafamostat might prefer only one orientation for DAO binding. We used in silico docking to predict amino acid interactions and the preferred orientation for nafamostat binding. Nafamostat docking resulted in 6 poses, 3 of them had a binding mode similar to the binding mode of diminazene in the crystal complex (PDB ID 3HIG). The aromatic rings of two similar poses with the docking scores of -7.893 and -6.910 superimposed well with those of diminazene in the DAO complex structure (Fig. 5A). In the crystal complex (Fig. 5B) the buried amidinium group of diminazene interacts with the catalytic Asp373, and the vicinal phenyl group pi-stacks with Tyr371 and Trp376. The nitrogen atoms in the triazine make hydrogen bonds with Asp186 and Tyr148. The Tyr148 residue also pi-stacks with the distal phenyl ring, which is clamped between Tyr148 and Phe435 from the other chain. The terminal amidinium forms a water-mediated hydrogen bond with Thr145. The binding site is surrounded by the hydrophobic Val458 and Ala149 residues and the aromatic residues Tyr459, Phe184 and Tyr152.

Based on the interaction analysis (Fig. 5C and 5D) the second-best pose for nafamostat showed more interactions than the best pose. Since it also showed a better calculated binding energy ΔG of -67.00 kcal/mol (the best post demonstrated a ΔG of -63.09 kcal/mol), the

JPET Fast Forward. Published on June 10, 2022 as DOI: 10.1124/jpet.122.001248
This article has not been copyedited and formatted. The final version may differ from this version.

second pose was selected as a representative binding mode for nafamostat. Like the buried amidinium in the diminazene crystal complex (Fig. 5B), the buried guanidino group in the second nafamostat pose (Fig. 5C) forms a salt bridge with a catalytic Asp373 and the vicinal phenyl group pi-stacks with Tyr371 and interacts with Trp376. Compared to amidinium the guanidinium group in nafamostat possesses an additional nitrogen, which makes both direct and water-mediated hydrogen bonds to Asn460. Like the phenyl group in diminazene, the naphtyl group in nafamostat pi-stacks with Tyr148 and interacts with Phe435 from the other chain. The central carbonyl group creates a hydrogen bond with Tyr148 and the distal amidinium interacts with Thr145 via a direct hydrogen bond and forms water-mediated hydrogen bonds with Tyr152 and Ala149. The predicted binding mode of nafamostat to DAO is highly similar to the binding mode of diminazene in the crystal complex with a preferred orientation of the guanidinium group towards the topaquinone.

JPET Fast Forward. Published on June 10, 2022 as DOI: 10.1124/jpet.122.001248
This article has not been copyedited and formatted. The final version may differ from this version.

Discussion

It is not surprising that nafamostat is a potent DAO inhibitor when one compares nafamostat to the structure of the known DAO inhibitors pentamidine and diminazene. In silico ligand docking studies revealed a remarkable similarity in amino acid interactions between nafamostat and diminazene. The K_i of diminazene using insect cell-derived DAO and putrescine was 14 nM and therefore quite similar to the 27 nM measured in our experiments (McGrath et al., 2009).

The 5-fold increased K_i for histamine (138 nM) compared to putrescine (27 nM) is likely a reflection of the 7-times lower K_m of histamine (2.8 μM) compared to putrescine (20 μM) for DAO (Elmore et al., 2002).We have seen similarly higher IC_{50} values for histamine compared to the simple diamines putrescine or cadaverine using other inhibitors (unpublished data). Nafamostat is clearly a potent DAO inhibitor in vitro, but the key question is whether DAO inhibition could be involved in the hypersensitivity reactions during nafamostat treatment and possibly also in effects currently ascribed to protease inhibition in animal models or clinical trials. Therefore, nafamostat inhibition of histamine degradation in plasma is more important and here we measured IC_{50} values of 2 to 3 μM using 180 nM histamine.

Normal histamine concentrations are below 0.5 ng/ml or 4.5 nM (Pollock et al., 1991). Histamine starts to induce symptoms such as flush and headache at less than 3 ng/ml, and significant hypotension develops above 5 ng/ml (Kaliner et al., 1982; Pollock et al., 1991). We could not test lower histamine concentrations in our DAO activity assays, but during severe anaphylaxis mean histamine concentrations of 140 ng/ml or 1260 nM have been measured and at this level 2 to 3 μM nafamostat would be sufficient to inhibit plasma DAO activity (Van der Linden et al., 1992). Table 2 summarizes published IC_{50} and K_i data for nafamostat using frequently pure buffer matrices or more than 5-fold diluted plasma samples.

JPET Fast Forward. Published on June 10, 2022 as DOI: 10.1124/jpet.122.001248
This article has not been copyedited and formatted. The final version may differ from this version.

Hitomi (1985) and Fujii (1981) published ratios of IC_{50} to K_i values of 0.68 and 0.39 respectively for prothrombin, which circulates at 1.4 µM (Fujii et al., 1981; Hitomi et al., 1985). In our case the ratio of IC_{50} using 90% plasma to K_i in buffer for histamine is 22-fold. Giardina et al. (2018) published an extrapolated IC_{50} shift for tryptase inhibition of at least 7-fold comparing buffer with >80% plasma (Supp. Fig. 6) (Giardina et al., 2018). Protease inhibition assays with nafamostat might show significantly higher IC_{50} values, indicating weaker potency of nafamostat using high plasma concentrations. Paques and Römisch used 75% plasma to test coagulation parameters and the K_i values seem higher compared to the other data in Table 2 (Paques and Römisch, 1991). Published nafamostat inhibition data are inconsistent (Table 2 and Supp. Table 2). What might be the reason for this strong shift in the plasma IC_{50} values when using plasma versus buffer?

We initially assumed that nafamostat is rapidly degraded by abundant plasma arylesterases but we were not able to find any effect of several arylesterase inhibitors on DAO inhibition using nafamostat (Yamaori et al., 2006). An alternative explanation would be that plasma proteins trap nafamostat and therefore the IC_{50} values increase. Table 2 lists the concentrations of nafamostat target proteases. The sum of the known nafamostat binding proteins is approximately 5 µM. Nafamostat might bind to these proteins with significant affinity before the proteases are activated.

In our assays we used maximally 12 nM DAO concentrations and therefore the ratio of all nafamostat binding proteins to DAO would be 417. This indicates that nafamostat binding to DAO competes with binding to 400-fold more abundant additional target proteins. Plasma DAO might be significantly inhibited at the high nafamostat concentrations used during hemodialysis or cardiopulmonary bypass operations with saturation of protease binding sites.

Some of the SARS-CoV-2 cell entry inhibition data have been performed with buffer or only 10% plasma. The relatively low IC_{50} values of 55 nM (Hempel et al., 2021) or 10 nM

JPET Fast Forward. Published on June 10, 2022 as DOI: 10.1124/jpet.122.001248
This article has not been copyedited and formatted. The final version may differ from this version.

(Yamamoto et al., 2020) might increase significantly using higher plasma concentrations, but irreversible binding likely follows different inhibition kinetics.

Normally, human DAO is not circulating but is present at high local concentrations in the extracellular matrix of the jejunum/ileum and renal proximal tubular epithelial cells (Boehm et al., 2017). Nevertheless, exogenous high molecular/unfractionated heparin is able to rapidly release DAO from the extracellular storage sites in the gastrointestinal tract (D'Agostino et al., 1988). During cardiopulmonary bypass operations with or without nafamostat treatment, heparin was used at 300 IU/kg and this amount of heparin very likely released endogenous DAO (Miyamoto et al., 1992; D'Agostino et al., 1988). Nafamostat, probably present at μM plasma concentrations during the cardiopulmonary bypass procedure, might have mediated inhibition of heparin-released plasma DAO and this inhibition could have caused the more than 5-fold difference in plasma histamine concentrations (Miyamoto et al., 1992).

Diamine oxidase is also released into plasma during severe anaphylaxis and mast cell activation events in both animals and humans (Rose and Leger, 1952; Code et al., 1961; Boehm et al., 2019). Therefore, nafamostat could cause anaphylaxis and mast cell activation events to deteriorate by blocking plasma DAO activity. Recombinant human DAO might also be developed as a new first-in-class biopharmaceutical for the treatment of anaphylaxis, mastocytosis, chronic urticaria or asthma exacerbations (Gludovacz et al., 2021). Co-administration of nafamostat might interfere with the potency of recombinant human DAO.

High concentrations of DAO are bound extracellularly to interstitial heparan sulfate proteoglycans in the gastro-intestinal tract and renal proximal tubular cells, but the role of DAO in the degradation of endogenous histamine released during anaphylaxis is not clear. Nevertheless, if the concentration of nafamostat in the interstitial fluid is high enough to efficiently inhibit local matrix-bound DAO, higher histamine concentrations are not only locally present after release from degranulating mast cells, but will also reach the circulation.

JPET Fast Forward. Published on June 10, 2022 as DOI: 10.1124/jpet.122.001248
This article has not been copyedited and formatted. The final version may differ from this version.

Locally and systemically elevated histamine levels will increase clinical symptom severity during anaphylaxis, mast cell activation syndrome, mastocytosis or chronic urticaria. Of the approximately 100 mg total histamine stored in the body, 50 and 30 percent are located within the granules of the mast cells in the gastrointestinal tract and the skin respectively. It is these organs which frequently demonstrate symptoms during hypersensitivity reactions (Boehm et al., 2021).

The interstitial fluid contains about 30% of the protein concentration compared to plasma (Supp. Table 1; Fogh-Andersen et al., 1995) and therefore simplified the concentration of nafamostat binding proteins might be only about 1.5 μM and this could increase the potency of nafamostat to inhibit local DAO activity in the gastrointestinal tract and kidneys.

What are the concentrations of nafamostat in the interstitial fluid or in the gastrointestinal tract and kidneys? The volume of distribution for nafamostat in healthy volunteers was described as 0.36 L/kg or 25 liters in a person weighing 70 kg, indicating that nafamostat is present at high concentrations in the interstitial fluid (Osono et al., 1991). The interstitial fluid compartment is about 3-times the plasma volume. In rats 15 minutes after intravenous infusion nafamostat rapidly accumulated in the kidneys and duodenum/jejunum (65- and 8- to 10-fold respectively compared to plasma). It might then be reabsorbed in the kidneys in the proximal tubules via organic cation transporters (Supp. Table 3 and Supp. Table 4) (Nanpo et al., 1984; Li et al., 2004). Pentamidine and furamidine, two diamidines with related chemical structures compared to nafamostat, are also transported via human organic cation transporters (Ming et al., 2009). Diamine oxidase is located in the extracellular matrix of renal proximal tubular and gastrointestinal epithelial cells. If humans show a similar accumulation of nafamostat when compared to rats, DAO might be potently inhibited by the high tissue concentrations of nafamostat. Nafamostat might compete with the transport of histamine into basophils or other cells. Histamine also uses organic cation transporters, and if high plasma

nafamostat concentrations interfere with histamine reabsorption into basophils, and possibly endothelial cells and other cells, the relative histamine exposure would increase (Schneider et al., 2005; Sakata et al., 2010).

Nafamostat is clearly associated with hypersensitivity reactions in humans but is there additional in vivo evidence of DAO inhibition and consequently of elevated histamine concentrations? High dose nafamostat administration in dogs, defined as plasma concentrations of more than 15 μM for 24 hours, caused the mean arterial pressure to drop statistically significantly after 6 hours, and remain low until the end of the infusions 18 hours later (Okamoto et al., 1994). The mean arterial pressure decrease was approximately 35%, from 125 to 80 mmHg. Diamine oxidase inhibition at these high nafamostat concentrations could have increased the circulating histamine levels and at least co-contributed to hypotension in dogs, which are sensitive to histamine (Owen et al., 1982).

Ceuleers et al. (2018) tested three nafamostat concentrations (0.1, 1 and 10 mg/kg) in a rat colitis model for irritable bowel syndrome. Tryptase, a biomarker for mast cells, was increased during inflammation, indicating the involvement of mast cells. Although nafamostat is a highly potent inhibitor for tryptase, only the lower nafamostat concentration showed beneficial effects in this model. Interestingly, experimental colitis in mice seems to be driven by histamine released from mast cells via histamine 4 receptor binding (Wechsler et al., 2018). We speculate that medium and high nafamostat concentrations not only inhibited tryptase, but also local DAO, thus resulting in elevated proinflammatory histamine concentrations counteracting the positive effects of tryptase inhibition.

In conclusion, nafamostat is a potent DAO inhibitor. During anaphylaxis or in general mast cell activation with massive release of histamine, concomitant nafamostat treatment might cause potent DAO inhibition leading to elevated histamine levels with possibly life-threatening consequences.

JPET Fast Forward. Published on June 10, 2022 as DOI: 10.1124/jpet.122.001248
This article has not been copyedited and formatted. The final version may differ from this version.

Acknowledgements

We gratefully acknowledge three diploma students, Julia Henkel, Linda Thurner and Marija Gorickic, for performing some of the experiments used in this publication. The library at the MUV was indispensable for providing literature. We also thank the bioinformatics (J.V. Lehtonen), translational activities and structural biology (FINStruct) infrastructure support from the Biocenter Finland and the computational infrastructure support from the CSC IT Center for Science at the Structural Bioinformatics Laboratory (SBL) of the Åbo Akademi University. The SBL is part of the NordForsk Nordic POP (Patient Oriented Products) and the Solutions for Health strategic area of the Åbo Akademi University. This research was supported by the InFLAMES Flagship Program of the Academy of Finland (decision number: 337530) and the Sigrid Juselius foundation. We are indebted to Sarah Ely for the final polish in the proper usage of the English language.

Authorship Contributions

Participated in research design: Boehm, Jilma

Conducted experiments: Petroczi, Gludovacz, Alix, Vakal

Performed data analysis: Boehm, Alix, Vakal, Salminen

Wrote or contributed to the writing of the manuscript: Boehm, Borth, Salminen, Jilma

References

Adasme MF, Linnemann KL, Bolz SN, Kaiser F, Salentin S, Haupt VJ, and Schroeder M (2021) PLIP 2021: expanding the scope of the protein-ligand interaction profiler to DNA and RNA. Nucleic Acids Res doi: 10.1093/nar/gkab294.

Aoyama T, Ino Y, Ozeki M, Oda M, Sato T, Koshiyama Y, Suzuki S, and Fujita M (1984) Pharmacological studies of FUT-175, nafamostat mesilate. I. Inhibition of protease activity in in vitro and in vivo experiments. Jpn J Pharmacol doi: 10.1254/jjp.35.203.

Asakura H, and Ogawa H (2020) Potential of heparin and nafamostat combination therapy for COVID-19. J Thromb Haemost doi: 10.1111/jth.14858.

Bardsley WG, Crabbe MJ, Shindler JS, and Ashford JS (1972) Oxidation of p-dimethylaminomethylbenzylamine by pig kidney diamine oxidase; A new method for spectrophotometric assay. Biochem J 127(5):875-9.

Boehm T, Karer M, Gludovacz E, Petroczi K, Resch R, Schuetzenberger K, Klavins K, Borth N, and Jilma B (2020) Simple, sensitive and specific quantification of diamine oxidase activity in complex matrices using newly discovered fluorophores derived from natural substrates. Inflamm Res doi: 10.1007/s00011-020-01359-5.

Boehm T, Pils S, Gludovacz E, Szoelloesi H, Petroczi K, Majdic O, Quaroni A, Borth N, Valent P, and Jilma B (2017) Quantification of human diamine oxidase. Clin Biochem doi: 10.1016/j.clinbiochem.2016.12.011.

Boehm T, Reiter B, Ristl R, Petroczi K, Sperr W, Stimpfl T, Valent P, and Jilma B (2019) Massive release of the histamine-degrading enzyme diamine oxidase during severe anaphylaxis in mastocytosis patients. Allergy doi: 10.1111/all.13663.

Boehm T, Ristl R, Joseph S, Petroczi K, Klavins K, Valent P, and Jilma B (2021) Metabolome and lipidome derangements during a severe mast cell activation event in a

patient with indolent systemic mastocytosis. J Allergy Clin Immunol doi: 10.1016/j.jaci.2021.03.043.

Ceuleers H, Hanning N, Heirbaut J, Van Remoortel S, Joossens J, Van Der Veken P, Francque SM, De Bruyn M, Lambeir AM, De Man TG, Timmermans JP, Augustyns K, De Meester I, and De Winter BY (2018) Newly developed serine protease inhibitors decrease visceral hypersensitivity in a post-inflammatory rat model for irritable bowel syndrome. Br J Pharmacol doi: 10.1111/bph.14396.

Code CF, Cody DT, Hurn M, Kennedy JC, and Strickland MJ (1961) The simultaneous release of histamine and a histamine-destroying factor during anaphylaxis in rats. J Physiol doi: 10.1113/jphysiol.1961.sp006669.

D'Agostino L, Daniele B, Pallone F, Pignata S, Leoni M, and Mazzacca G (1988) Postheparin plasma diamine oxidase in patients with small bowel Crohn's disease. Gastroenterology doi: 10.1016/s0016-5085(88)80069-6.

Duch DS, Bacchi CJ, Edelstein MP, and Nichol CA (1984) Inhibitors of histamine metabolism in vitro and in vivo: correlations with antitrypanosomal activity. Biochem Pharmacol 33(9):1547-1553.

Elmore BO, Bollinger JA, and Dooley DM (2002) Human kidney diamine oxidase: heterologous expression, purification, and characterization. J Biol Inorg Chem doi: 10.1007/s00775-001-0331-1.

Fogh-Andersen N, Altura BM, Altura BT, and Siggaard-Andersen O (1995) Composition of interstitial fluid. Clin Chem 41(10):1522-5.

Fujii S, and Hitomi Y (1981) New synthetic inhibitors of C1r, C1 esterase, thrombin, plasmin, kallikrein and trypsin. Biochim Biophys Acta doi: 10.1016/0005-2744(81)90023-1.

Giardina SF, Werner DS, Pingle M, Bergstrom DE, Arnold LD, and Barany F (2018) A novel, nonpeptidic, orally active bivalent inhibitor of human β-tryptase. Pharmacology doi:10.1159/000492078.

Gludovacz E, Schuetzenberger K, Resch M, Tillmann K, Petroczi K, Schosserer M, Vondra S, Vakal S, Klanert G, Pollheimer J, Salminen TA, Jilma B, Borth N, and Boehm T (2021) Heparin-binding motif mutations of human diamine oxidase allow the development of a first-in-class histamine-degrading biopharmaceutical. Elife doi: 10.7554/eLife.68542.

Han SJ, Kim HS, Kim KI, Whang SM, Hong KS, Lee WK, and Lee SH (2011) Use of nafamostat mesilate as an anticoagulant during extracorporeal membrane oxygenation. J Korean Med Sci doi: 10.3346/jkms.2011.26.7.945.

Hempel T, Raich L, Olsson S, Azouz NP, Klingler AM, Hoffmann M, Pöhlmann S, Rothenberg ME, and Noe F (2021) Molecular mechanism of inhibiting the SARS-CoV-2 cell entry facilitator TMPRSS2 with camostat and nafamostat. Chem Sci doi: 10.1039/D0SC05064D.

Hitomi Y, Ikari N, and Fujii S (1985) Inhibitory effect of a new synthetic protease inhibitor (FUT-175) on the coagulation system. Haemostasis doi: 10.1159/000215139.

Hoffmann M, Schroeder S, Kleine-Weber H, Müller MA, Drosten C, and Pöhlmann S (2020) Nafamostat mesylate blocks activation of SARS-CoV-2: New treatment option for COVID-19. Antimicrob Agents Chemother doi: 10.1128/AAC.00754-20.

Janes SM, Palcic MM, Scaman CH, Smith AJ, Brown DE, Dooley DM, Mure M, and Klinman JP (1992) Identification of topaquinone and its consensus sequence in copper amine oxidases. Biochemistry doi: 10.1021/bi00163a025.

Kaliner M, Shelhamer JH, and Ottesen EA (1982) Effects of infused histamine: correlation of plasma histamine levels and symptoms. J Allergy Clin Immunol 69:283-289.

Khersonsky O, and Tawfik DS (2005) Structure-reactivity studies of serum paraoxonase PON1 suggest that its native activity is lactonase. Biochemistry doi: 10.1021/bi047440d.

Kim HS, Lee KE, Oh JH, Jung CS, Choi D, Kim Y, Jeon JS, Han DC, and Noh H (2016) Cardiac arrest caused by nafamostat mesilate. Kidney Res Clin Pract doi: 10.1016/j.krcp.2015.10.003.

Kim JH, Park JY, Jang SH, Kim JK, Song YR, Lee HS, and Kim SG (2021) Fatal anaphylaxis due to nafamostat mesylate during hemodialysis. Allergy Asthma Immunol Res doi: 10.4168/aair.2021.13.3.517.

Li Q, Sai Y, Kato Y, Muraoka H, Tamai I, and Tsuji A (2004) Transporter-mediated renal handling of nafamostat mesilate. J Pharm Sci doi: 10.1002/jps.10534.

Maruyama H, Miyakawa Y, Gejyo F, and Arakawa M (1996) Anaphylactoid reaction induced by nafamostat mesilate in a hemodialysis patient. Nephron doi: 10.1159/000189371.

McGrath AP, Caradoc-Davies T, Collyer CA, and Guss JM (2010) Correlation of active site metal content in human diamine oxidase with trihydroxyphenylalanine quinone cofactor biogenesis. Biochemistry doi: 10.1021/bi1010915.

McGrath AP, Hilmer KM, Collyer CA, Shepard EM, Elmore BO, Brown DE, Dooley DM, and Guss JM (2009) Structure and inhibition of human diamine oxidase. Biochemistry 48:9810-9822.

Midgley I, Hood AJ, Proctor P, Chasseaud LF, Irons SR, Cheng KN, Brindley CJ, and Bonn R (1994) Metabolic fate of ^{14}C-camostat mesylate in man, rat and dog after intravenous administration. Xenobiotica doi: 10.3109/00498259409043223.

Minakata D, Fujiwara SI, Ikeda T, Kawaguchi SI, Toda Y, Ito S, Ochi SI, Nagayama T, Mashima K, Umino K, Nakano H, Yamasaki R, Morita K, Kawasaki Y, Sugimoto M, Yamamoto C, Ashizawa M, Hatano K, Sato K, Oh I, Ohmine K, Muroi K, Ohmori T, and

Kanda Y (2019) Comparison of gabexate mesilate and nafamostat mesilate for disseminated intravascular coagulation associated with hematological malignancies. Int J Hematol doi: 10.1007/s12185-018-02567-w.

Ming X, Ju W, Wu H, Tidwell RR, Hallo JE, and Thakker DR (2009) Transport of dicationic drugs pentamidine and furamidine by human organic cation transporters. Drug Metab Dispos doi: 10.1124/dmd.108.024083.

Miyamoto Y, Nakano S, Kaneko M, Takano H, and Matsuda H (1992) Clinical evaluation of a new synthetic protease inhibitor in open heart surgery. Effect on plasma serotonin and histamine release and blood conservation. ASAIO J doi: 10.1097/00002480-199207000-00063.

Mori S, Itoh Y, Shinohata R, Sendo T, Oishi R, and Nishibori M (2003) Nafamostat mesilate is an extremely potent inhibitor of human tryptase. J Pharmacol Sci doi: 10.1254/jphs.92.420.

Nanpo T, Ohtsuki T, Jin Y, Matsunaga K, Takahashi M, Shibuya M, Sasaki H, and Kurumi M (1984) Pharmacokinetic study of FUT-175 (nafamostat mesilate). (1) Blood level profiles, tissue distribution, metabolism and excretion in rats after intravenous administration. Clin Rep 1984;18:467–488.

Novotny WF, Chassande O, Baker M, Lazdunski M, and Barbry P (1994) Diamine oxidase is the amiloride-binding protein and is inhibited by amiloride analogues. J Biol Chem 269(13):9921-5.

Okajima K, Uchiba M, and Murakami K (1995) Nafamostat mesilate. Cardiovasc Drug Rev doi: 10.1111/j.1527-3466.1995.tb00213.x.

Okamoto T, Mizoguchi S, Terasaki H, and Morioka T (1994) Safety of high-dose of nafamostat mesilate: toxicological study in beagles. J Pharmacol Exp Ther 268(2):639-44.

Ookawara S, Ito K, and Morishita Y (2018) Sustained deterioration of hepatic oxygenation after nafamostat mesilate-induced anaphylactic shock during hemodiafiltration. Artif Organs doi: 10.1111/aor.13097.

Osono E, Takeuchi M, Kitamura H, Matsunobu S, Komaba Y, Aoyama T, Kawabe M, Arai T, Lino Y, Hara K, and Terashi A (1991) Pharmacokinetics of nafamostat mesilate (FUT) in patients undergoing hemodialysis. Dialysis J 24(1):49-53. (Article in Japanese)

Owen DA, Harvey CA, and Boyce MJ (1982) Effects of histamine on the circulatory system. Klin Wochenschr doi: 10.1007/BF01716957.

Paques EP, and Römisch J (1991) Comparative study on the in vitro effectiveness of antithrombotic agents. Thromb Res doi: 10.1016/0049-3848(91)90201-7.

Pollock I, Murdoch RD, and Lessof MH (1991) Plasma histamine and clinical tolerance to infused histamine in normal, atopic and urticarial subjects. Agents Actions doi: 10.1007/BF01980899.

Rose B, and Leger J (1952) Serum histaminase during rabbit anaphylaxis. Proc Soc Exp Biol Med doi: 10.3181/00379727-79-19386.

Russell DH (1983) Clinical relevance of polyamines. Crit Rev Clin Lab Sci 18(3):261-311.

Sakamoto T, Kano H, Miyahara S, Inoue T, Izawa N, Gotake Y, Matsumori M, Okada K, and Okita Y (2014) Efficacy of nafamostat mesilate as anticoagulation during cardiopulmonary bypass for early surgery in patients with active infective endocarditis complicated by stroke. J Heart Valve Dis 23(6):744-51.

Sakata T, Anzai N, Kimura T, Miura D, Fukutomi T, Takeda M, Sakurai H, and Endou H (2010) Functional analysis of human organic cation transporter OCT3 (SLC22A3) polymorphisms. J. Pharmacol Sci doi: 10.1254/jphs.09331sc.

Sattler J, Häfner D, Klotter HJ, Lorenz W, and Wagner PK (1988) Food-induced histaminosis as an epidemiological problem: plasma histamine elevation and haemodynamic alterations after oral histamine administration and blockade of diamine oxidase (DAO). Agents Actions 23:361-5.

Sawada K, Ohdo M, Ino T, Nakamura T, Numata T, Shibata H, Sakou J, Kusada M, and Hibi T (2016) Safety and tolerability of nafamostat mesilate and heparin as anticoagulants in leukocytapheresis for Ulcerative Colitis: Post hoc analysis of a large-scale, prospective, observational study. Ther Apher Dial doi: 10.1111/1744-9987.12357.

Schneider E, Machavoine F, Pleau JM, Bertron AF, Thurmond OL, Ohtsu H, Watanabe T, Schinkel AH, and Dy M (2005) Organic cation transporter 3 modulates murine basophil functions by controlling intracellular histamine levels. J Exp Med doi: 10.1084/jem.20050195.

Schwelberger HG, Hittmair A, and Kohlwein SD (1998a) Analysis of tissue and subcellular localization of mammalian diamine oxidase by confocal laser scanning fluorescence microscopy. Inflamm Res doi: 10.1007/s000110050273.

Schwelberger HG, Stalzer B, Maier H, and Bodner E (1998b) Expression and cellular localization of diamine oxidase in the gastrointestinal tract of pigs. Inflamm Res doi: 10.1007/s000110050275.

Sjaastad ÖV (1967) Potentiation by aminoguanidine of the sensitivity of sheep to histamine given by mouth. Effect of aminoguanidine on the urinary excretion of endogenous histamine. Q J Exp Physiol Cogn Med Sci 52:319–330.

Southren AL, Kobayashi Y, Sherman DH, Levine L, Gordon G, and Weingold AB (1964) Diamine oxidase in human pregnancy: Plasma diamine oxidase in nonpregnant and normal pregnant patients. Am J Obst Gynecol 89:199-203.

Van der Linden PW, Hack CE, Poortman J, Vivie-Kipp YC, Struyvenberg A, and Van der Zwan JK (1992) Insect-sting challenge in 138 patients: relation between clinical severity of anaphylaxis and mast cell activation. J Allergy Clin Immunol 90:110-118.

Velicky P, Windsperger K, Petroczi K, Pils S, Reiter B, Weiss T, Vondra S, Ristl R, Dekan S, Fiala C, Cantonwine DE, McElrath TF, Jilma B, Knöfler M, Boehm T, and Pollheimer J (2018) Pregnancy-associated diamine oxidase originates from extravillous trophoblasts and is decreased in early-onset preeclampsia. Sci Rep doi: 10.1038/s41598-018-24652-0.

Wechsler JB, Szabo A, Hsu CL, Krier-Burris RA, Schroeder HA, Wang MY, Carter RG, Velez TE, Aguiniga LM, Brown JB, Miller ML, Wershil BK, Barrett TA, and Bryce PJ (2018) Histamine drives severity of innate inflammation via histamine 4 receptor in murine experimental colitis. Mucosal Immunol doi: 10.1038/mi.2017.121.

Yamamoto M, Kiso M, Sakai-Tagawa Y, Iwatsuki-Horimoto K, Imai M, Takeda M, Kinoshita N, Ohmagari N, Gohda J, Semba K, Matsuda Z, Kawaguchi Y, Kawaoka Y, and Inoue JI (2020) The anticoagulant nafamostat potently inhibits SARS-CoV-2 S protein-mediated fusion in a cell fusion assay system and viral infection in vitro in a cell-type-dependent manner. Viruses doi: 10.3390/v12060629.

Yamaori S, Fujiyama N, Kushihara M, Funahashi T, Kimura T, Yamamoto I, Sone T, Isobe M, Ohshima T, Matsumura K, Oda M, and Watanabe K (2006) Involvement of human blood arylesterases and liver microsomal carboxylesterases in nafamostat hydrolysis. Drug Metab Pharmacokinet doi: 10.2133/dmpk.21.147.

No author has an actual or perceived conflict of interest with the contents of this article.

Footnotes

This work did not receive any specific grant from funding agencies in the public, commercial, or not-for-profit sectors.

JPET Fast Forward. Published on June 10, 2022 as DOI: 10.1124/jpet.122.001248
This article has not been copyedited and formatted. The final version may differ from this version.

Fig. 1. Nafamostat is a potent recombinant human DAO inhibitor

(A) Nafamostat inhibits DAO activity using H_2O_2-HRP luminol coupling. One µg/ml purified DAO was incubated with 200 µM putrescine and different concentrations of various DAO inhibitors in PBS containing 0.1% human serum albumin. The specific luminescence signals at 60 min were compared to DAO without inhibitors (100% DAO activity); Grey circles = AML; White triangles (Δ) = PHL; Black squares (■) = NAF; White diamonds (◊) = DAZ; The means of duplicates are shown; **(B)** Nafamostat inhibits direct deamination of p-dimethylaminomethylbenzylamine. Aldehyde generation using 1 µg/ml rhDAO was measured using specific absorption rate changes at 250 nm; The same inhibitors as in (A) including BZL were tested at 1 and 10 µM; The means (+/- SEM) of duplicate determinations of two independent experiments are shown; **(C)** Nafamostat efficiently blocks the generation of delta-1-piperideine. Fusion of ortho-aminobenzaldehyde with the DAO oxidation product of cadaverine, autocyclized delta-1-piperideine, was measured using fluorescence; The slopes in the linear range were compared with different NAF concentrations and normalized to control DAO activity; The means (+/- SEM) of two independent experiments in duplicate are shown; **(D)** Camostat is a weak DAO inhibitor. One, 3.3 and 10 µM CAM or Foipan tablets dissolved in DMSO (FOI) or water (FOI_H) were tested in the same assay as in (C); The means of duplicates are shown; AML= amiloride; PHL = phenamil; BZL = benzamil; NAF = nafamostat; DAZ = diminazene aceturate; CAM = camostat; FOI = Foipan tablet dissolved in DMSO; FOI_H = Foipan tablet dissolved in water.

JPET Fast Forward. Published on June 10, 2022 as DOI: 10.1124/jpet.122.001248
This article has not been copyedited and formatted. The final version may differ from this version.

Fig. 2. Nafamostat is a reversible DAO inhibitor and pH independent at physiologically relevant pH values.

(A) Nafamostat is not an irreversible DAO inhibitor. Purified DAO was immobilized on a microtiter plate pre-coated with a monoclonal anti-DAO antibody and incubated with various inhibitors at 10 μM; After 30 min at 37°C, the plates were washed and DAO activity was measured using H_2O_2-HRP vanillic acid/4-aminoantipyrine coupling; noAB = no anti-DAO antibody coating; DAO = control wells without inhibitor; DAZ = diminazene aceturate; AMG = aminoguanidine (irreversible DAO inhibitor); PHY = phenylhydrazine (irreversible DAO inhibitor) and NAF = nafamostat; The means of duplicate determinations are shown; **(B)** The mean (+/-SEM) specific absorption at 60 min of 3 independent experiments as presented in (A) are summarized with n = 3 for control DAO activity (Con; 100%), NAF and DAZ and n = 1 for AMG, PHY and MHY (methylhydrazine; irreversible DAO inhibitor); For AMG, PHY and MHY the SDs of the duplicates are shown; **(C)** Relative DAO inhibition by NAF is equal between pH 6 and 8. The Britton Robinson buffer system was used to measure DAO activity between pH 6 and 10. White squares (□) represent DAO control oxidation rates corresponding to the slopes of chromophore accumulation using H_2O_2-HRP vanillic acid/4-aminoantipyrine coupling; Data using NAF at 1 μM are presented using black circles (●). NAF inhibition as percent of DAO activity is shown on the second y-axis (black triangles; ▲); **(D)** The Chemicalize software estimated a pKa of 7.6 for the guanidine moiety of NAF. The three curves were generated using the Henderson-Hasselbalch equation. Percent acid represents percent deprotonation of the guanidine moiety of NAF at different pKa values.

JPET Fast Forward. Published on June 10, 2022 as DOI: 10.1124/jpet.122.001248
This article has not been copyedited and formatted. The final version may differ from this version.

Fig. 3. Kinetic analysis of DAO inhibition by nafamostat.

(A) Different putrescine concentrations were incubated with various nafamostat concentrations shown below Panels A and B; DAO activity was measured using the highly sensitive H_2O_2-HRP Amplex red coupling and corresponds to the linear part of the slope of fluorescence curves; **(B)** Same as in (A) using different histamine concentrations. K_i values were determined using GraphPad; the curves in (A) and (B) represent the means of duplicate determinations; **(C; D)** V_{max} (white squares □) and K_m (black triangles ▲) values using different nafamostat and putrescine (C) or histamine (D) concentrations; The error bars correspond to the standard error; **(E)** Calculated IC_{50} values are plotted versus putrescine concentrations; **(F)** Same as in (E) for histamine; K_i, K_m and V_{max} data and mode of inhibition are summarized in Table 1.

JPET Fast Forward. Published on June 10, 2022 as DOI: 10.1124/jpet.122.001248
This article has not been copyedited and formatted. The final version may differ from this version.

Fig. 4. Nafamostat inhibition of DAO activity in human EDTA plasma.

In Panels A and B fusion of ortho-aminobenzaldehyde with autocyclized delta-1-piperideine, the cadaverine (CAD) DAO oxidation product, was measured using fluorescence; **(A)** 85% EDTA plasma was incubated for 1 hour at 37°C with 0.4 µg/ml purified DAO in the absence and presence of different nafamostat concentrations using 200 µM CAD (white triangles Δ; n = 1) and 20 µM CAD (black circles ●; n = 4) as indicated. Specific fluorescence was normalized to control DAO samples. The means (+/- coefficient of variation for 200 µM CAD and +/-SD for 20 µM CAD) of duplicate determinations are shown. **(B)** Similar conditions to Panel A but incubation was only performed for 30 min at 37°C; DNT = 5,5'-dithiobis(2-nitrobenzoic acid) or Ellman's reagent was used at 1 mM; Eth means 5% ethanol (DNT solvent); C_P means control plasma and D_P means DNT directly dissolved in control plasma at 2 mM; Only 80% plasma was used in the Eth and DNT samples; The numbers after the sample abbreviations are IC_{50} concentrations; The means of duplicates of single donors for each set (ethanol as solvent with and without DNT versus direct dissolution of DNT in plasma) are shown; **(C and D)** 90% EDTA plasma was spiked with 1 µg/ml (6 nM) purified DAO and 100 ng/ml (0.9 µM) or 20 ng/ml (0.18 µM) histamine in the absence and presence of different nafamostat concentrations. After 1 hour incubation at 37°C the remaining histamine was quantified using the Cisbio HTRF histamine assay; The means (+/-SD) of 4 different plasma samples from healthy volunteers are shown in Panels C and D; Histamine measurements were performed in duplicate; DAO activity in the absence of nafamostat was set to 100%.

JPET Fast Forward. Published on June 10, 2022 as DOI: 10.1124/jpet.122.001248
This article has not been copyedited and formatted. The final version may differ from this version.

Fig. 5. Molecular docking of nafamostat to the active site of DAO compared with the diminazene/DAO crystal structure.

All atomic interactions are presented based on the results from the PLIP webserver (Adasme et al., 2021)**.** The side chains for the residues in chain A within 4Å from the binding site are shown as violet lines in Panel A and as sticks in Panels B to D. Phe435 from chain B is purple; (A) Diminazene (light red) in complex with DAO (PDB ID 3HIG, red) superimposed with the two best poses of docked nafamostat (light and dark blue); (B) The interactions between diminazene (red) and DAO in the crystal complex; (C) The interactions between the best pose of nafamostat (light blue) docking with DAO; (D) The interactions between the second best pose of nafamostat (dark blue) docking with DAO.

JPET Fast Forward. Published on June 10, 2022 as DOI: 10.1124/jpet.122.001248
This article has not been copyedited and formatted. The final version may differ from this version.

TABLE 1 Nafamostat is a mixed mode inhibitor of human DAO using putrescine and histamine as substrates

	PUT MM Inh	SE	L 95% CI	U 95% CI	HIS MM Inh	SE	L 95% CI	U 95% CI
V_{max}	23111	1381	20309	25912	10126	463	9185	11066
K_i nM	27	12	3	50	138	25	87	190
K_m µM	3.1	1.1	0.9	5.3	2.8	0.34	2.1	3.5
Adj. R^2	0.926				0.986			
Alpha	12.1				4.9			
ExSOS F	MM vs	C	0.0022				0.0006	
		NonC	0.0018				0.0003	
		UnC	0.0001				0.0001	

PUT = Putrescine; HIS = Histamine; Inh = Inhibitor; L = Lower; U = Upper; ExSOS F = Extra sum-of-squares F test; SE = Standard Error; Adj. = Adjusted; CI = Confidence Interval; MM = Mixed mode inhibition; C = Competitive; NonC = Non-competitive; UnC = Un-competitive inhibition.

JPET Fast Forward. Published on June 10, 2022 as DOI: 10.1124/jpet.122.001248
This article has not been copyedited and formatted. The final version may differ from this version.

TABLE 2 Nafamostat binding proteins in competition with DAO binding

NBP	[Plasma] µM	IC_{50} Hitomi (1985)	K_i Hitomi (1985)	IC_{50} Fujii (1981)	K_i Fujii (1981)	IC_{50} Aoyama (1984)	K_i Paques (1991)	IC_{50} Giardina (2018)
PK	0.24	3.0E-09		3.1E-07		3.9E-06	1.2E-08	2.0E-10
Plg	2.2	1.0E-07		4.1E-07		1.2E-07	3.7E-06	3.7E-09
PT	1.4	8.8E-07	1.3E-06	3.3E-07	8.4E-07	1.9E-06	4.9E-06	2.3E-07
FXII	0.44	3.3E-07					1.1E-07	
FX	0.13	2.1E-06	4.1E-06				1.2E-04	8.8E-07
C1r	0.39			2.1E-07	1.4E-08	8.0E-07		
C1s	0.41			5.1E-08	3.8E-08	2.9E-08		
Sum	5.2							

The following data are from this study						
[DAO]* µg/ml	[DAO]* µM	Ki PUT	Ki HIS	IC_{50} PUT**	IC_{50} PUT**	IC_{50} CAD**
0.4	0.0048	2.7E-08	1.4E-07	4.1E-07	3.4E-07	3.2E-07
1	0.012					

The different plasma protease activities have been measured after generation of active proteases; Nafamostat binding data to the not-activated enzyme precursors are not available; *DAO concentrations used in this study; **200 µM substrate concentration; NBP = potential Nafamostat Binding Protein; PK = Pre-Kallikrein; Plg = Plasminogen; PT = Prothrombin; FXII = Factor XII; C1r and C1s = Complement component 1r and 1s; HIS = Histamine; PUT = Putrescine; CAD = Cadaverine; IC_{50} = Inhibitory concentration 50%; K_i = Inhibitor constant.

JPET Fast Forward. Published on June 10, 2022 as DOI: 10.1124/jpet.122.001248
This article has not been copyedited and formatted. The final version may differ from this version.

Figure 1

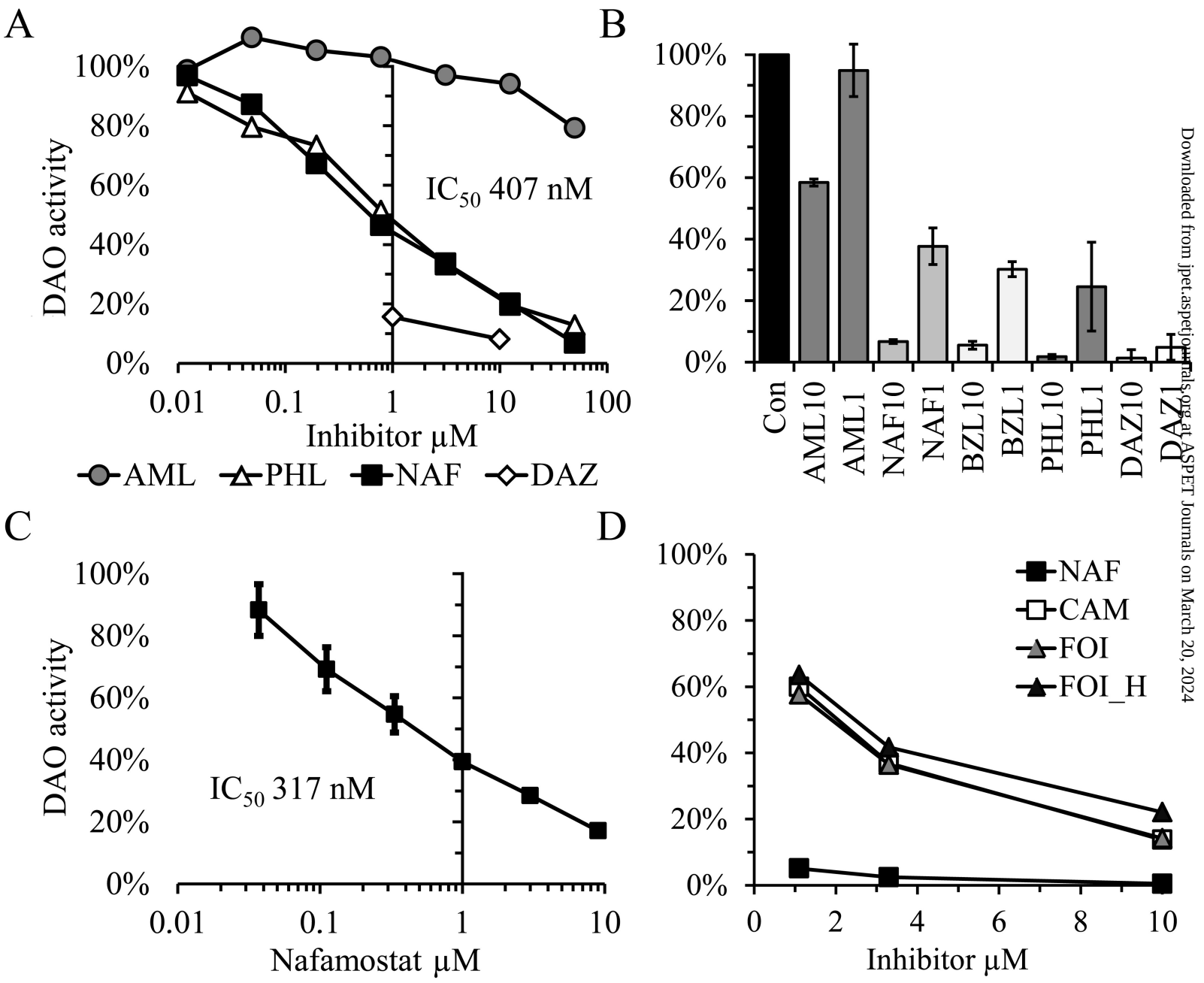

JPET Fast Forward. Published on June 10, 2022 as DOI: 10.1124/jpet.122.001248
This article has not been copyedited and formatted. The final version may differ from this version.

Figure 2

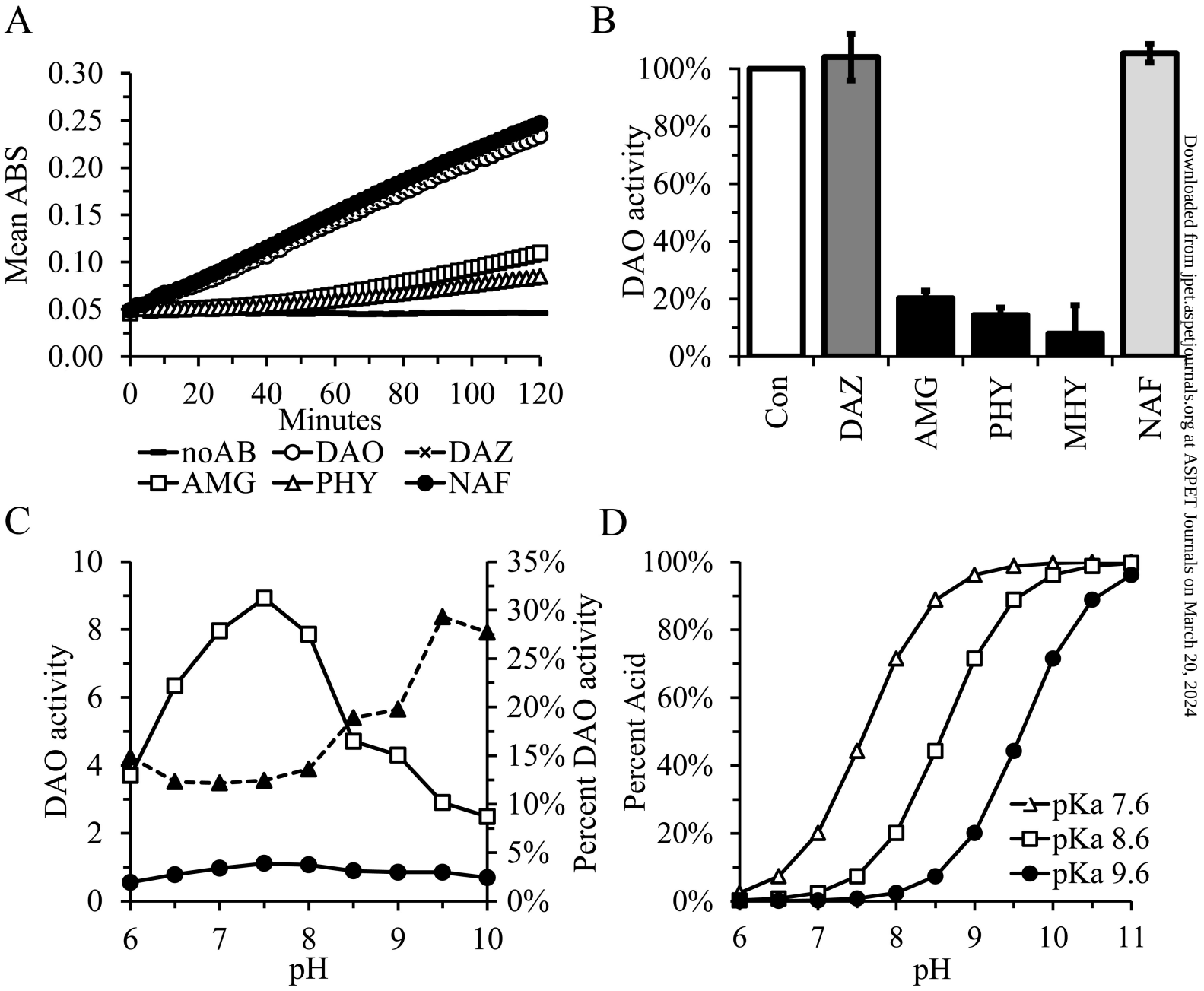

Figure 3

JPET Fast Forward. Published on June 10, 2022 as DOI: 10.1124/jpet.122.001248

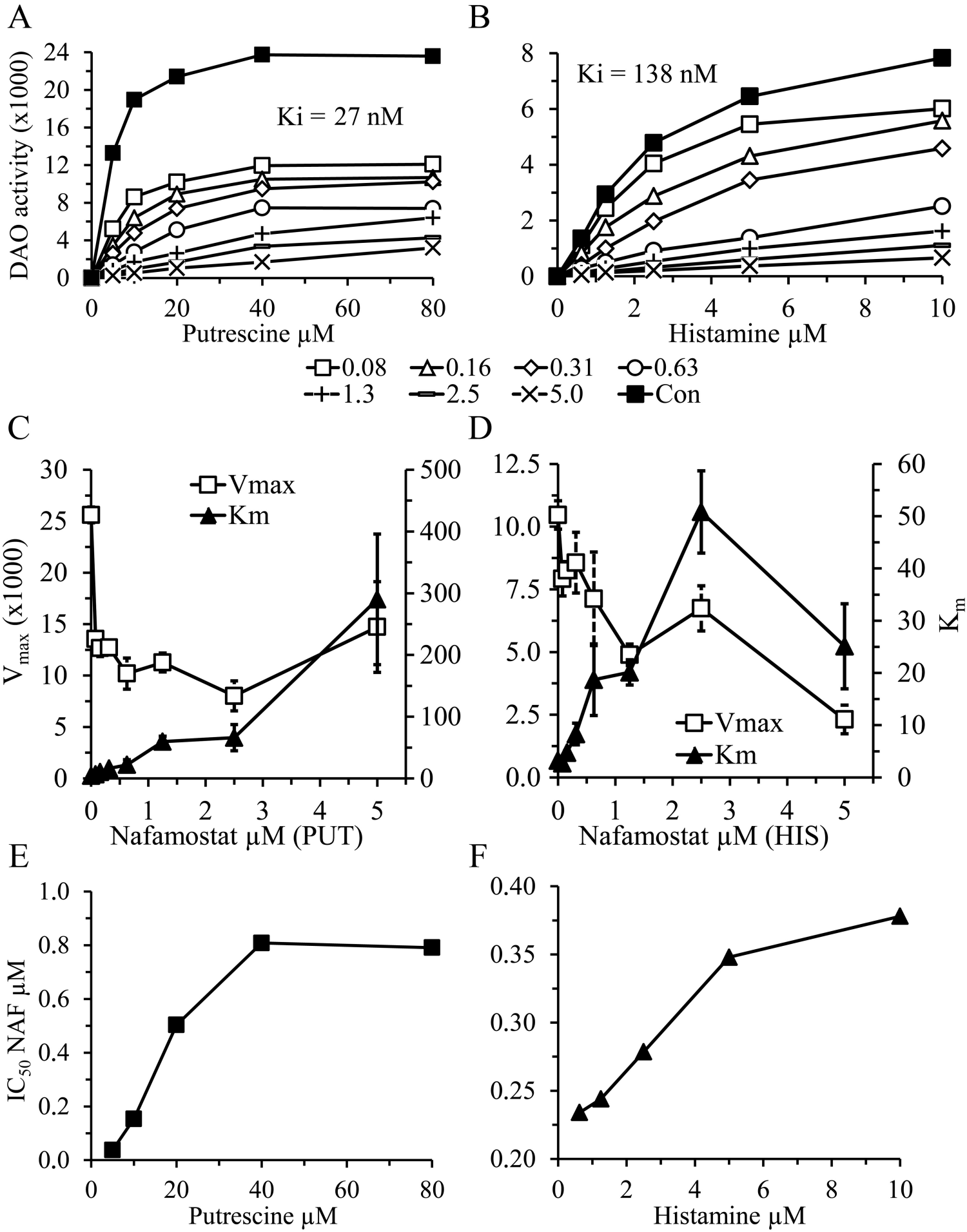

JPET Fast Forward. Published on June 10, 2022 as DOI: 10.1124/jpet.122.001248
This article has not been copyedited and formatted. The final version may differ from this version.

Figure 4

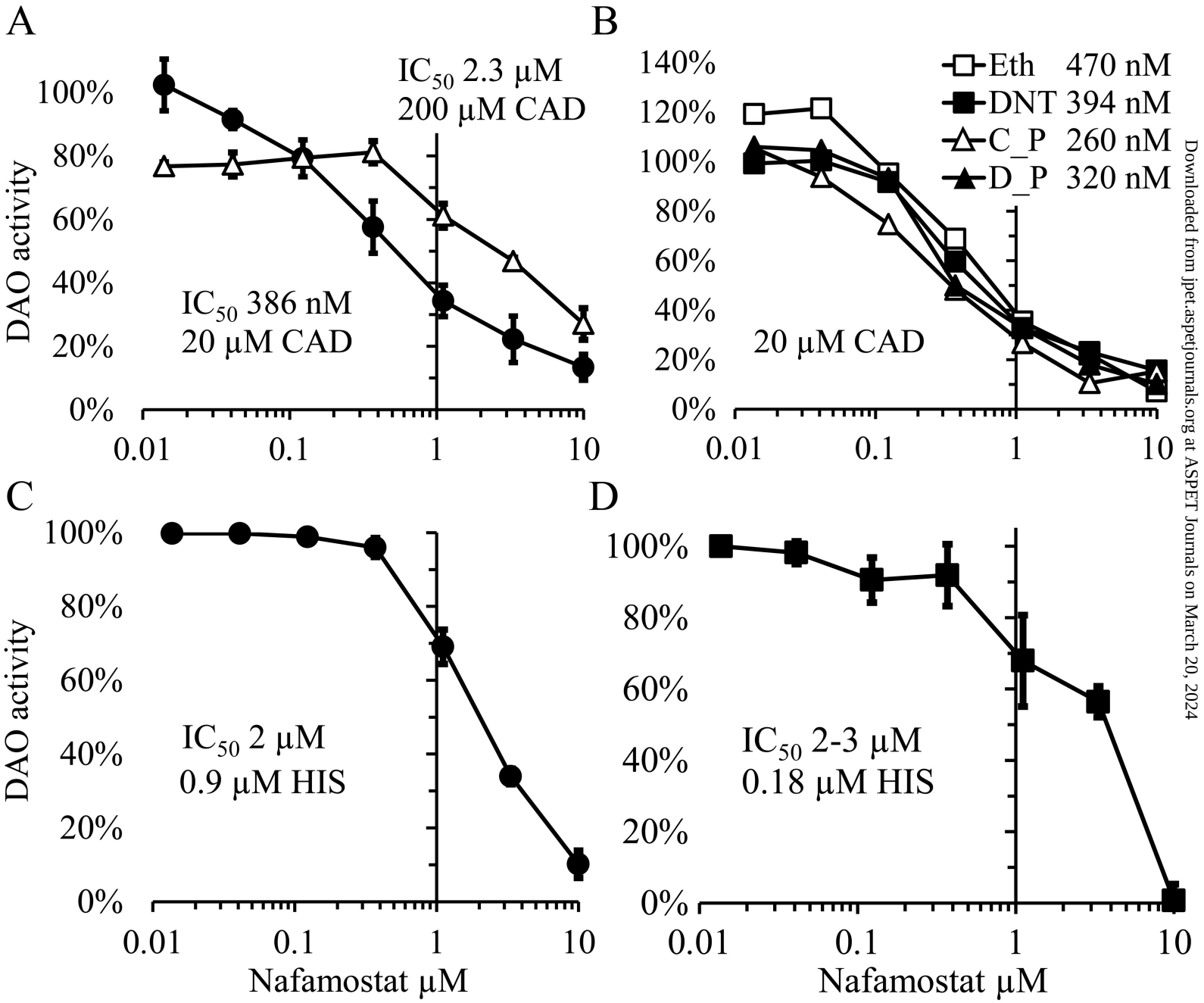

Figure 5

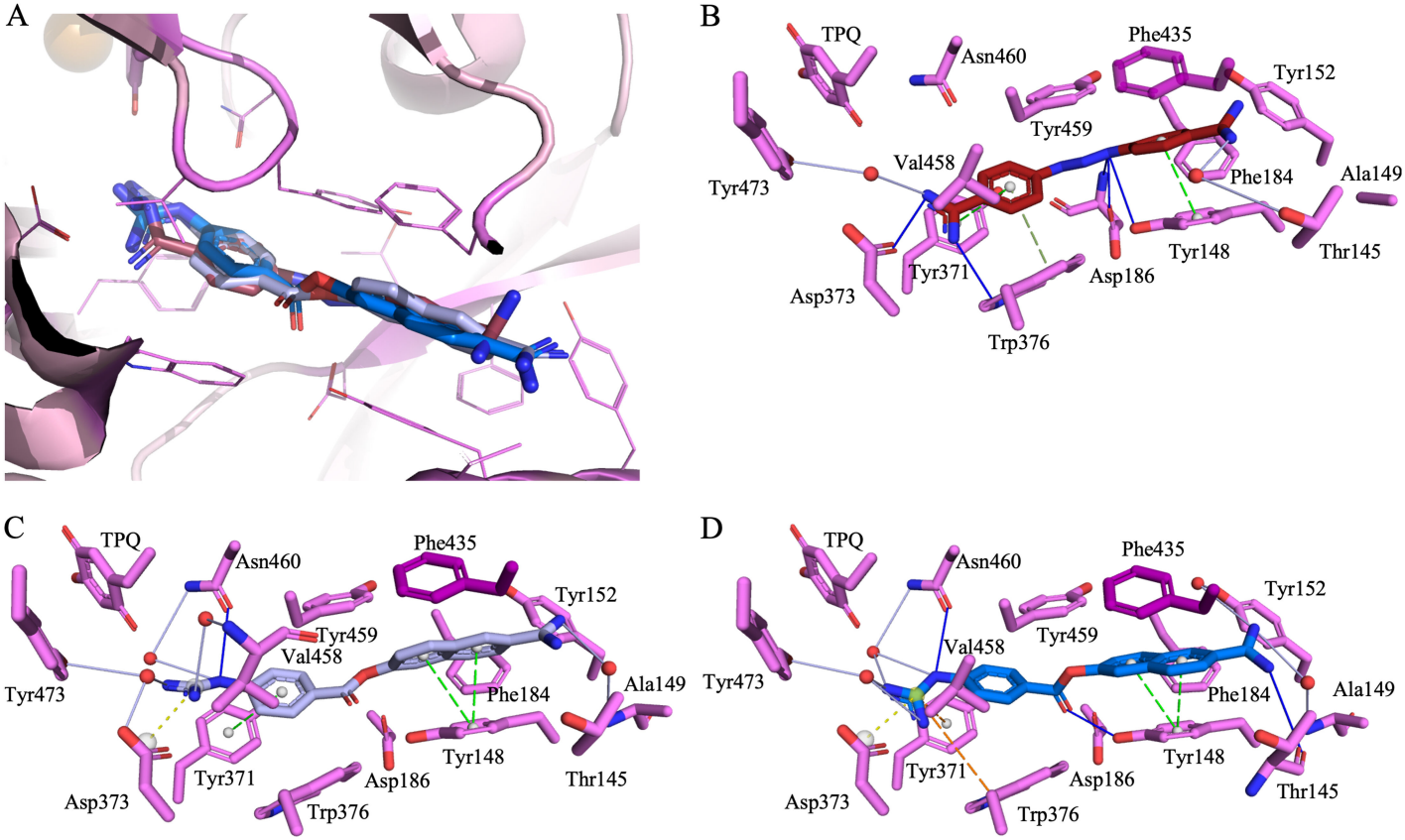
A
B
TPQ
Asn460
Phe435
Tyr152
Tyr459
Val458
Tyr473
Phe184
Ala149
Tyr148
Thr145
Tyr371
Asp186
Asp373
Trp376
C
TPQ
Asn460
Phe435
Tyr152
Tyr459
Val458
Tyr473
Phe184
Ala149
Tyr148
Tyr371
Asp186
Thr145
Asp373
Trp376
D
TPQ
Asn460
Phe435
Tyr152
Tyr459
Val458
Tyr473
Phe184
Ala149
Tyr148
Tyr371
Asp186
Thr145
Asp373
Trp376